Proceedings of the
Annual Stability Conference
Structural Stability Research Council
Orlando, Florida, April 12-15, 2016

GBT-Based Buckling Analysis of Circular Cylindrical Steel Shells under Uniform External Pressure

Cilmar Basaglia[1], Dinar Camotim[2], Nuno Silvestre[3], Leandro Palermo Jr.[1]

Abstract

This paper reports the results of an investigation on the use of Generalized Beam Theory (GBT) to assess the buckling behavior of circular cylindrical steel shells (pipes and pressure vessels) subject to uniform external pressure. Initially, a novel formulation based on GBT is derived, which (i) incorporates all the effects stemming from the presence of longitudinal and/or hoop stresses (the latter are stresses acting in the circumferential direction), and (ii) taking into account the destabilizing effects associated with the follower nature of the external pressure (it remains normal to the shell wall before and after deformation). Then, after the above formulation is numerically implemented by means of GBT-based beam finite elements method, results concerning the buckling behavior of tubes and pressure vessels under external pressure are presented and discussed, in order to illustrate the application and capabilities of the proposed GBT-based approach. For validation purposes, most GBT results are compared with values either available in the literature or yielded by ANSYS shell finite element analyses.

1. Introduction

Many pressure vessels and undersea or underground pipelines typically used in the mechanical and petroleum industries are formed by circular cylindrical steel shells. However, since these structures often exhibit slender cross-sections (walls), they are highly susceptible to buckling phenomena, particularly when subject to external pressure (Annaratone 2007).

Various approaches have been used to assess the buckling behavior of circular cylindrical shells under hydrostatic external pressure. Probably the most popular of such approaches consists of using the energy method to determine the critical buckling pressure (Arjomandi 2010). On the other hand, analytical solutions to obtain the critical buckling pressure were first developed and presented by Bryan (1889), for long tubes, and by von Mises (1929) and Nash (1954), for short pressure vessels or tubes (including tubes reinforced by circumferential rings) – however, the major difficulty associated with the development of closed form solution stems from the (i) need to consider arbitrary boundary conditions and (ii) mathematical determination of the number of lobes, *i.e.*, the number of circumferential waves associated with the buckling mode. It is also worth mentioning the numerical investigations carried out by Brendel & Ramm (1980), Vodenitcharova & Ansourian (1996), Karamanos & Tassoulas (1996),

[1] FEC, DES, University of Campinas, <cbasaglia@fec.unicamp.br>, <leandro@fec.unicamp.br>
[2] CERIS, ICIST, DECivil, Instituto Superior Técnico, Universidade de Lisboa, Portugal. <dcamotim@civil.ist.utl.pt>
[3] LAETA, IDMEC, DEM, Instituto Superior Técnico, Universidade de Lisboa, Portugal. <nsilvestre@ist.utl.pt>

Rasheed & Yousif (2005), Cao & Zhao (2010), Paor *et al.* (2012). Finally, an interesting state-of-the-art review on the buckling and collapse of offshore pipelines was published a few years ago by Kyriakides & Corona (2007).

The numerical assessment of the structural response of circular cylindrical steel shells under hydrostatic external pressure constitutes a complex task. Indeed, rigorous numerical analyses can only be performed by resorting to shell finite element models (*e.g.*, Ross 2011) – however, this is a time-consuming approach still prohibitive for routine applications. Moreover, the differential equation governing the adjacent equilibrium of a shell structure acted by external pressure loading must take into account the follower nature of such loading, *i.e.*, the fact that it changes direction during the shell deformation, in order to remain always normal to the shell wall. In this context, it is worth pointing out the works of Hibbitt (1979), Iwata *et. al*. (1991) and Paimushin (2008), who developed approaches in which the external pressure follower effects are incorporated into the shell buckling eigenvalue problem through a "loading matrix" (in addition to the conventional linear and geometrically non-linear stiffness matrices).

Even if there are several results available in the literature (*e.g.*, Boresi 1955, Bodner 1958 and Iwata *et. al* 1991) showing that disregarding the external pressure follower effects may lead to overestimations of pipe critical buckling pressures by amounts that can exceed *30*%, several commercial finite element software packages still include shell finite elements not equipped to conduct an accurate eigenvalue buckling analysis for shells subject to follower pressure[4] – for instance, this is the case of the widely popular SHELL63 element belonging to the code ANSYS (SAS 2009) library.

In order to render the buckling analysis of steel pressure vessels and pipelines undergoing external pressure simpler and more accessible, without sacrificing too much the accuracy of the results obtained, it is mandatory to develop easy-to-use numerical tools based on beam finite element models. A very promising approach is Generalized Beam Theory (GBT), a thin-walled prismatic bar theory that incorporates genuine plate/shell concepts, *i.e.*, accounts for cross-section in- and out-of plane deformation. Moreover, the unique GBT modal nature leads to very elegant and illuminating solutions for a wealth of structural problems. In this context, Silvestre (2007) developed a GBT formulation specifically aimed at investigating the buckling behavior of circular hollow section members subjected to compression, bending and/or torsion.

The objective of this work is to present the development and numerical implementation, and illustrate the application of a novel GBT formulation to analyze the buckling behavior of circular cylindrical steel shells subjected to uniform external pressure. This formulation incorporates (i) geometrical stiffness terms associated with the internal work done by the pre-buckling longitudinal and hoop stresses, and (ii) non-linear terms associated with the follower nature of the external (lateral) pressure. Initially, thin-shell kinematics are employed to derive the virtual work done by the internal forces (stresses) and follower external pressure, and also to provide the mechanical interpretation of its terms. Next, the formulation and numerical implementation of a GBT-based beam finite element are presented. Finally, the buckling behavior of thin-walled steel pipes and pressure vessels undergoing uniform external pressure is investigated. For validation purposes, some GBT results are compared with values either available in the literature or obtained by means of ANSYS shell finite element analyses.

2. GBT Formulation

Because the cross-section displacement field is expressed as a linear combination of structurally meaningful deformation modes, GBT analyses involve solving equilibrium equation systems written in

[4] Moreover, such software packages do not even provide information warning against this deficiency.

a very convenient modal form, which lead to solutions providing in-depth insight on the member structural response under consideration. The performance of a buckling analysis involves (i) a *cross-section analysis*, to obtain the deformation modes and corresponding mechanical properties, and (ii) a *member analysis*, *i.e.*, the solution of the buckling eigenvalue problem followed by the (modal) interpretation of the results determined (critical loads and buckling mode shapes).

Figure 1 depicts a prismatic member with a circular hollow section, having radius r and wall thickness t, and the global coordinate system X, Y, Z. In order to account for the cross-section in-plane deformation effects, it is preferable to consider the local coordinate system x, θ, z, (a longitudinal coordinate $x \in [0;L]$, an angular coordinate $\theta \in [0;2\pi]$ and a thickness coordinate $z \in [-t/2; +t/2]$) – u,v,w are the displacement components expressed in the local coordinate systems. According to the Love-Kirchoff assumptions, the relations between the displacement components of an arbitrary point P (u^P, v^P, w^P), lying on a member wall, and the corresponding mid-plane ($z=0$) point P_0 (u, v, w) are expressed by (Schardt 1989)

$$u^P = u - z w_{,x} \qquad v^P = \left(1 + \frac{z}{r}\right) v - \frac{z}{r} w_{,\theta} \qquad w^P = w \quad , \quad (1)$$

where $(.)_{,x} \equiv d(.)/dx$. In order to obtain a displacement field representation compatible with the classical beam theory, each displacement component (u, v or w) at any given point of the cross-section mid-surface must be expressed as a combination of orthogonal functions. Therefore, one has

$$u(x,\theta) = u_k(\theta)\phi_{k,x}(x) \qquad v(x,\theta) = v_k(\theta)\phi_k(x) \qquad w(x,\theta) = w_k(\theta)\phi_k(x) \quad , \quad (2)$$

where (i) the summation convention applies to subscript k and (ii) $u_k(\theta)$, $v_k(\theta)$ and $w_k(\theta)$ are functions characterizing deformation mode k (Silvestre 2007). Since the thin-walled member is deemed made of an isotropic elastic material (*e.g.*, constructional steel), the constitutive relation reads

$$\begin{Bmatrix} \sigma_{xx} \\ \sigma_{\theta\theta} \\ \tau_{x\theta} \end{Bmatrix} = \begin{bmatrix} \frac{E}{1-\nu^2} & \frac{E\nu}{1-\nu^2} & 0 \\ \frac{E\nu}{1-\nu^2} & \frac{E}{1-\nu^2} & 0 \\ 0 & 0 & G \end{bmatrix} \begin{Bmatrix} \varepsilon_{xx} \\ \varepsilon_{\theta\theta} \\ \gamma_{x\theta} \end{Bmatrix} = \begin{bmatrix} Q_{11} & Q_{12} & 0 \\ Q_{21} & Q_{22} & 0 \\ 0 & 0 & Q_{33} \end{bmatrix} \begin{Bmatrix} \varepsilon_{xx} \\ \varepsilon_{\theta\theta} \\ \gamma_{x\theta} \end{Bmatrix} \quad , \quad (3)$$

where (i) E, G and ν are Young's modulus, shear modulus and Poisson's ratio and (ii) σ_{ij}, ε_{ij}, γ_{ij} are the plane stress and strain components.

According to the Sanders' non-linear theory of shells (Sanders 1963), the strain components ε_{xx}, $\varepsilon_{\theta\theta}$ and $\gamma_{x\theta}$ at an arbitrary shell point are related to (i) their mid-surface counterparts, ε^0_{xx}, $\varepsilon^0_{\theta\theta}$ and $\gamma^0_{x\theta}$, and (ii) the mid-surface changes in bending curvature and torsion, κ_{xx}, $\kappa_{\theta\theta}$ and $\kappa_{x\theta}$, by the relations

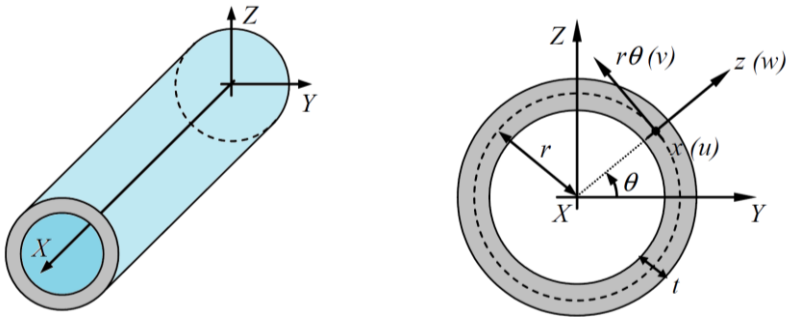

Figure 1: Circular hollow section member and global and local coordinate system and displacement components.

$$\varepsilon_{xx} = \varepsilon_{xx}^0 + z\kappa_{xx} = u_{,x} + \frac{1}{2}\beta_x^2 + \frac{1}{2}\beta^2 + z\kappa_{xx} \tag{4}$$

$$\varepsilon_{\theta\theta} = \varepsilon_{\theta\theta}^0 + z\kappa_{\theta\theta} = \frac{v_{,\theta} + w}{r} + \frac{1}{2}\beta_\theta^2 + \frac{1}{2}\beta^2 + z\kappa_{\theta\theta} \tag{5}$$

$$\gamma_{x\theta} = \gamma_{x\theta}^0 + z\kappa_{x\theta} = \frac{u_{,\theta}}{r} + v_{,x} + \beta_x\beta_\theta + z\kappa_{x\theta} \quad , \tag{6}$$

where

$$\beta_x = -w_{,x} \qquad \beta_\theta = \frac{v - w_{,\theta}}{r} \qquad \beta = \frac{1}{2}\left(v_{,x} - \frac{u_{,\theta}}{r}\right) \tag{7}$$

$$\kappa_{xx} = \beta_{x,x} \qquad \kappa_{\theta\theta} = \frac{1}{r}\beta_{\theta,\theta} \qquad \kappa_{x\theta} = \frac{1}{r}\beta_{x,\theta} + \beta_{\theta,x} + \frac{1}{r}\beta \quad . \tag{8}$$

By incorporating (7) and (8) into (4) to (6), one obtains

$$\varepsilon_{xx} = u_{,x} + \frac{1}{2}w_{,x}^2 + \frac{1}{8}\left(v_{,x} - \frac{u_{,\theta}}{r}\right)^2 - zw_{,xx} \tag{9}$$

$$\varepsilon_{\theta\theta} = \frac{v_{,\theta} + w}{r} + \frac{1}{2}\left(\frac{v - w_{,\theta}}{r}\right)^2 + \frac{1}{8}\left(v_{,x} - \frac{u_{,\theta}}{r}\right)^2 - z\frac{w_{,\theta\theta} - v_{,\theta}}{r^2} \tag{10}$$

$$\gamma_{x\theta} = \frac{u_{,\theta}}{r} + v_{,x} + w_{,x}\left(\frac{w_{,\theta} - v}{r}\right) - z\left(\frac{4rw_{,x\theta} - 3rv_{,x} + u_{,\theta}}{2r^2}\right) \quad . \tag{11}$$

The incorporation of expressions (2) into (9) to (11) leads to the linear and non-linear (^{NL}) kinematical (strain-displacement) relations given by

$$\varepsilon_{xx} = u_k\phi_{k,xx} - zw_k\phi_{k,xx} \tag{12}$$

$$\varepsilon_{\theta\theta} = \frac{v_{k,\theta} + w_k}{r}\phi_k - z\frac{w_{k,\theta\theta} - v_{k,\theta}}{r^2}\phi_k \tag{13}$$

$$\gamma_{x\theta} = \left(\frac{u_{k,\theta}}{r} + v_k\right)\phi_{k,x} - z\left(\frac{4rw_{k,\theta} - 3rv_k + u_{k,\theta}}{2r^2}\right)\phi_{k,x} \tag{14}$$

$$\varepsilon_{xx}^{NL} = \frac{1}{2}w_k w_i\phi_{k,x}\phi_{i,x} + \frac{1}{8}\left(v_k - \frac{u_{k,\theta}}{r}\right)\left(v_i - \frac{u_{i,\theta}}{r}\right)\phi_{k,x}\phi_{i,x} \tag{15}$$

$$\varepsilon_{\theta\theta}^{NL} = \frac{1}{2}\left(\frac{v_k - w_{k,\theta}}{r}\right)\left(\frac{v_i - w_{i,\theta}}{r}\right)\phi_k\phi_i + \frac{1}{8}\left(v_k - \frac{u_{k,\theta}}{r}\right)\left(v_i - \frac{u_{i,\theta}}{r}\right)\phi_{k,x}\phi_{i,x} \tag{16}$$

$$\gamma_{x\theta}^{NL} = w_k\left(\frac{w_{i,\theta} - v_i}{r}\right)\phi_{k,x}\phi_i \quad . \tag{17}$$

2.1 Equilibrium equations

When performing buckling analyses of thin-walled members, such as cylinders and pipes, the application of the Principle of Virtual Work, leading to the member equilibrium equations, reads

$$\delta W_{int} + \delta W_{ext} = \delta W^{L} + \delta W^{NL} + \delta W_{ext} = 0 \quad , \quad (18)$$

where (i) δW_{int} is the work done by the internal forces (pre-buckling stresses) on the virtual strains, which can still subdivided in two additive parts, namely the works done on the strains stemming from linear (δW^{L}) and non-linear (δW^{NL}) terms of the strain-displacement relations, and (ii) δW_{ext} is the (path-dependent) work done by follower external pressure on the cylinder/pipe wall virtual displacements[5].

2.1.1 Work done by the internal forces – δW_{int}

Since the main objective of the formulation is to analyze the buckling behavior of cylinders and pipes subjected to external pressure, the non-linear shear strain component $\gamma_{x\theta}^{NL}$ is disregarded from now on. In fact, the inclusion of this strain component is only needed in the context of the buckling analysis of members subjected to torsion, which is not the case in this work. Then, the work done by the internal forces (pre-buckling stresses) on the virtual strains is given by

$$\delta W_{int} = \delta W^{L} + \delta W^{NL} = \int_{L} \oint \int_{t} (\sigma_{xx}\delta\varepsilon_{xx} + \sigma_{\theta\theta}\delta\varepsilon_{\theta\theta} + \tau_{x\theta}\delta\gamma_{x\theta} + \sigma_{xx}^{0}\delta\varepsilon_{xx}^{NL} + \sigma_{\theta\theta}^{0}\delta\varepsilon_{\theta\theta}^{NL})\, dz r d\theta dx \quad , \quad (19)$$

where (i) L, r and t are the member length, cross-section mid-surface radius and thickness, respectively, and (ii) σ_{xx}^{0} and $\sigma_{\theta\theta}^{0}$ are the pre-buckling longitudinal stresses and hoop stresses (or stresses acting in the circumferential direction) caused by the applied external pressure p^0 – see Figure 2. Thus, one has either

$$\sigma_{xx}^{0} = \frac{p^0 r}{2t} \qquad \sigma_{\theta\theta}^{0} = \frac{p^0 r}{t} \quad , \quad (20)$$

if the external pressure acts on the shell lateral and end surfaces (*e.g.*, in cylinders and tanks with flat end surfaces), or

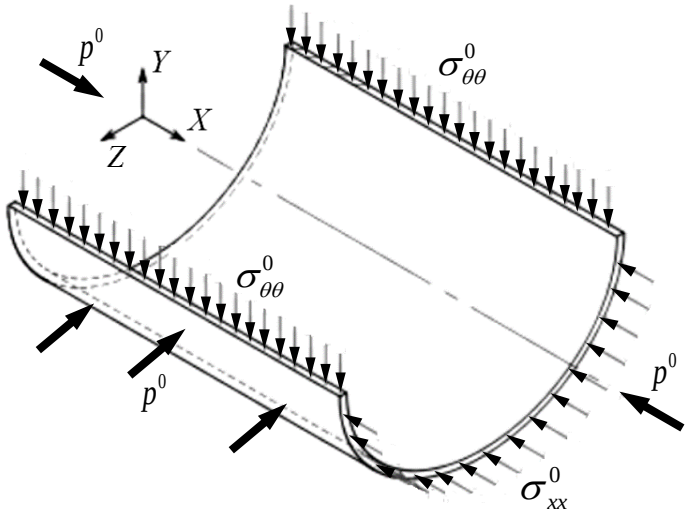

Figure 2: Pre-buckling longitudinal σ_{xx}^{0} and hoop $\sigma_{\theta\theta}^{0}$ stresses caused by the applied external pressure p^0.

[5] Since the shell material behaviour is linear elastic, δW_{int} can also be viewed as the first variation of the shell strain energy.

$$\sigma_{xx}^0 = 0 \qquad \sigma_{\theta\theta}^0 = \frac{p^0 r}{t} \quad , \quad (21)$$

if only the shell lateral surface is loaded (*e.g.*, in pipes).

Taking into account (i) the displacement approximations (2), (ii) the isotropic elastic constitutive relations (3) and (iii) the kinematic relations (12)-(16), it is possible to rewrite the works done by the internal forces on the strains due to the linear and non-linear strain-displacement relation terms as

$$\delta W^L = \int_L (C_{ik}\phi_{k,xx}\delta\phi_{i,xx} + D_{ik}^1\phi_{k,x}\delta\phi_{i,x} + D_{ik}^2\phi_k\delta\phi_{i,xx} + D_{ki}^2\phi_{k,xx}\delta\phi_i + B_{ik}\phi_k\delta\phi_i)dx \quad (22)$$

$$\delta W^{NL} = \int_L (X_{jik}^{\sigma xx}\phi_{k,x}\delta\phi_{i,x} + X_{jik}^{1\sigma\theta\theta}\phi_k\delta\phi_i + X_{jik}^{2\sigma\theta\theta}\phi_{k,x}\delta\phi_{i,x})dx \quad . \quad (23)$$

The tensors appearing in (22) and (23), which stem from the integration over the cross-section of displacement components and their derivatives, are defined by

$$C_{ik} = A_{11}\oint (u_k u_i)rd\theta + F_{11}\oint (w_k w_i)rd\theta \quad (24)$$

$$D_{ik}^1 = A_{33}\oint \left(\frac{u_{k,\theta}}{r} + v_k\right)\left(\frac{u_{i,\theta}}{r} + v_i\right)rd\theta + F_{33}\oint \left(\frac{4rw_{k,\theta} - 3rv_k + u_{k,\theta}}{2r^2}\right)\left(\frac{4rw_{i,\theta} - 3rv_i + u_{i,\theta}}{2r^2}\right)rd\theta \quad (25)$$

$$D_{ik}^2 = A_{12}\oint \left(\frac{v_{k,\theta} + w_k}{r}\right)u_i rd\theta + F_{12}\oint \left(\frac{w_{k,\theta\theta} - v_{k,\theta}}{r^2}\right)w_i rd\theta \quad (26)$$

$$B_{ik} = A_{22}\oint \left(\frac{v_{k,\theta} + w_k}{r}\right)\left(\frac{v_{i,\theta} + w_i}{r}\right)rd\theta + F_{22}\oint \left(\frac{w_{k,\theta\theta} - v_{k,\theta}}{r^2}\right)\left(\frac{w_{i,\theta\theta} - v_{k,\theta}}{r^2}\right)rd\theta \quad (27)$$

$$X_{jik}^{\sigma xx} = \oint \sigma_{xx}^0 \left(w_k w_i + \frac{1}{4}\left(v_k - \frac{u_{k,\theta}}{r}\right)\left(v_i - \frac{u_{i,\theta}}{r}\right)\right)trd\theta \quad (28)$$

$$X_{jik}^{1\sigma\theta\theta} = \oint \sigma_{\theta\theta}^0 \left(\frac{v_k - w_{k,\theta}}{r}\right)\left(\frac{v_i - w_{i,\theta}}{r}\right)trd\theta \quad X_{jik}^{2\sigma\theta\theta} = \oint \sigma_{\theta\theta}^0 \left(\frac{1}{4}\left(v_k - \frac{u_{k,\theta}}{r}\right)\left(v_i - \frac{u_{i,\theta}}{r}\right)\right)trd\theta \quad , \quad (29)$$

where it is worth noticing that $A_{ij}=Q_{ij}t$ and $F_{ij}=Q_{ij}t^3/12$ are membrane and flexural stiffness components. The pre-buckling longitudinal (σ_{xx}^0) and hoop ($\sigma_{\theta\theta}^0$) stresses appearing in (28)-(29) read[6]

$$\sigma_{xx}^0 = Q_{11}u_j\phi_{j,xx}^0 \quad (30)$$

$$\sigma_{\theta\theta}^0 = Q_{22}\left(\frac{v_{j,\theta} + w_j}{r}\right)\phi_j^0 \quad (31)$$

and their resultants (*i.e.*, the longitudinal and lateral loads) are

[6] Since the objective of this work is to analyze the buckling behavior of steel (isotropic) shell structures, the pre-buckling stresses stemming from strains caused by Poisson's effects are neglected here.

$$W_j^{\sigma xx} = C_{jj}\phi_{j,xx}^0 \tag{32}$$

$$W_j^{\sigma\theta\theta} = B_{jj}\phi_j^0 \quad . \tag{33}$$

2.1.2 Work done by the follower external pressure – δW_{ext}

According to Paimushin (2008), the (pre-buckling) follower external pressure is defined by the vector

$$\vec{\mathrm{p}}^0 = -p^0\vec{\mathrm{m}} = -p^0(E_1\hat{\mathrm{i}} + E_2\hat{\mathrm{j}} + E_3\hat{\mathrm{k}}) \tag{34}$$

where (i) $\hat{\mathrm{i}}$, $\hat{\mathrm{j}}$ and $\hat{\mathrm{k}}$ are orthonormal cartesian base vectors and (ii) components E_1, E_2 and E_3 read

$$E_1 = -w_{,x} + v_{,x}\frac{w_{,\theta} - v}{r} - w_{,x}\frac{v_{,\theta} + w}{r} \tag{35}$$

$$E_2 = -\frac{w_{,\theta} - v}{r} + \frac{u_{,\theta}}{r}w_{,x} - u_{,x}\frac{w_{,\theta} - v}{r} \tag{36}$$

$$E_3 = 1 + u_{,x} + \frac{v_{,\theta} + w}{r} + u_{,x}\frac{v_{,\theta} + w}{r} - v_{,x}\frac{u_{,\theta}}{r} \quad . \tag{37}$$

The work done by the external pressure on the virtual displacement is given by

$$\delta W_{ext} = \int_L \oint \int_t (\vec{\mathrm{p}}^0 \cdot \delta\vec{\mathrm{u}})\, dzrd\theta dx \quad , \tag{38}$$

where the virtual displacement is equal to

$$\delta\vec{\mathrm{u}} = \delta u\hat{\mathrm{i}} + \delta v\hat{\mathrm{j}} + \delta w\hat{\mathrm{k}} \quad . \tag{39}$$

Incorporating (34) into (38) and performing the scalar product, one obtains

$$\delta W_{ext} = -\int_L \oint \int_t p^0(E_1\delta u + E_2\delta v + E_3\delta w)\, dzrd\theta dx \quad . \tag{40}$$

Considering only the constant terms in Eqs. (35)-(37) (*i.e.*, E_1=E_2=0 and E_3=1), Eq. (40) takes the form

$$\delta W_{ext} = -\int_L \oint \int_t p^0(\delta w)\, dzrd\theta dx \quad , \tag{41}$$

corresponding to a conservative ("dead") pressure, whose direction remains unchanged (*i.e.*, does not vary with the wall deformation).

If only the constant and linear terms of E_1, E_2 and E_3 are considered, the δW_{ext} takes the form

$$\delta W_{ext} = -\int_L \oint \int_t p^0\left(-w_{,x}\delta u - \frac{w_{,\theta} - v}{r}\delta v + \left(1 + u_{,x} + \frac{v_{,\theta} + w}{r}\right)\delta w\right) dzrd\theta dx \quad . \tag{42}$$

According to Paimushin (2008), if it is assumed that (i) the rotations are small-to-moderate, (ii) the pressure applied to the shell/tank end cross-sections remains invariant in direction and (iii) the non-

conservative part of the overall end load does not perform work on the possible displacements (*e.g.*, in the linear buckling analysis of pipes or thin-walled tanks with thick end caps), the work done by the follower (lateral) external pressure can be deemed to consist only of the *linear* non-conservative parts associated with the terms E_1 and E_2 – therefore, one has

$$\delta W_{ext} = -\int_L \oint_t \int p^0 \left(-w_{,x}\delta u - \frac{w_{,\theta} - v}{r}\delta v \right) dz r d\theta dx \quad . \quad (43)$$

Taking into account the displacement approximations (2), it is possible to rewrite the work done by the follower lateral external pressure as

$$\delta W_{ext} = \int_L (H^1_{ik}\phi_{k,x}\delta\phi_{i,x} + H^2_{ik}\phi_k\delta\phi_i)dx \quad , \quad (44)$$

where

$$H^1_{ik} = \oint p^0 w_k u_i t r d\theta \quad (45)$$

$$H^2_{ik} = \oint p^0 \left(\frac{w_{k,\theta} - v_k}{r} \right) v_i t r d\theta \quad . \quad (46)$$

3. Deformation Modes

The cross-section analysis, performed to obtain the deformation modes and corresponding mechanical properties, comprises a set of sequential operations already described in detail by Schardt (1989), Silvestre (2007) and Basaglia *et al.* (2015). Nevertheless, it is worth drawing the reader's attention to the following aspects, concerning the concepts and procedures involved:

(i) The deformation modes consist of a "*shell-type*" mode family (those originally considered by Schardt 1986), an *axisymmetric* mode, a *torsion* mode (both first introduced by Silvestre 2007) and (warping) *shear modes* (initially introduced by Basaglia *et al.* 2015).

(ii) Like the conventional deformation modes of unbranched open cross-sections (*e.g.*, Bebiano *et al.* 2015), the "*shell-type*" modes, based on the assumption of null membrane shear strains $\gamma_{x\theta}$ and transverse extensions $\varepsilon_{\theta\theta}$, constitute the core of the GBT analysis of circular hollow section members. The displacement profiles of mode k are defined by (different expressions for even and odd k values)

$$m \geq 1, \quad k = 2m, \quad u_{2m} = r\sin(m\theta), \quad v_{2m} = -m\cos(m\theta), \quad w_{2m} = -m^2\sin(m\theta)$$

$$m \geq 1, \quad k = 2m+1, \quad u_{2m+1} = r\cos(m\theta), \quad v_{2m+1} = -m\sin(m\theta), \quad w_{2m+1} = -m^2\cos(m\theta) \quad , \quad (47)$$

where m is the number of circumferential waves exhibited by the trigonometric functions. Note that (ii$_1$) for a given m there are two similar modes with distinct order k, (ii$_2$) $m=0$ corresponds to the axial extension mode $k=1$ ($u_1=1$, $v_1=0$ and $w_1=0$) and (ii$_3$) any given $m>0$ corresponds to two similar deformation modes with distinct (consecutive) orders k. Figure 3 shows the in-plane deformed configurations of the first *14* shell-type modes.

(iii) The *axisymmetric* mode (identified by subscript **a**) involves only in-plane displacements and accounts for the cross-section deformation due to the extension in the circumferential direction – thus, the corresponding displacement profile is characterized by $u_a=0$, $v_a=0$ and $w_a=1$ (see Fig. 4).

(iv) The *torsion* mode (identified by subscript **t**) has a displacement profile characterized by $u_a=0$, $v_a=r$ and $w_a=0$ (see Fig. 4).

(v) The *shear* modes (identified by subscript **s**) involve only warping displacements – the displacement profiles of mode k are defined by (the expressions are different for even and odd k values). Figure 5 shows the warping displacements of the 8 shear modes (k=**1s**,…,**8s**)

$$m \geq 1, \quad k = 2m, \quad u_{2m} = r\sin(m\theta), \quad v_{2m} = 0, \quad w_{2m} = 0$$

$$m \geq 1, \quad k = 2m+1, \quad u_{2m+1} = r\cos(m\theta), \quad v_{2m+1} = 0, \quad w_{2m+1} = 0 \qquad . \quad (48)$$

(vi) It is worth noting that, unlike in flat-walled cross-sections (*e.g.*, Bebiano *et al.* 2015), the GBT cross-section analysis of a circular hollow section does not need to be related to a "physical (nodal) discretization" (*i.e.*, no node grid has to be defined before performing the cross-section analysis). Instead, the cross-section discretization is associated with the number of circumferential waves considered to define the shell-type deformation modes (*i.e.*, the m value).

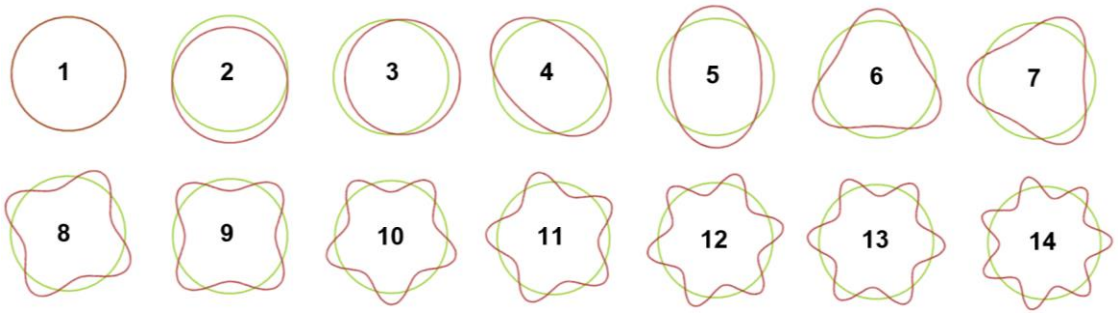

Figure 3: First *14* shell-type deformation modes for circular hollow cross-sections.

Figure 4: Axisymmetric (**a**) and (b) torsion (**t**) deformation modes.

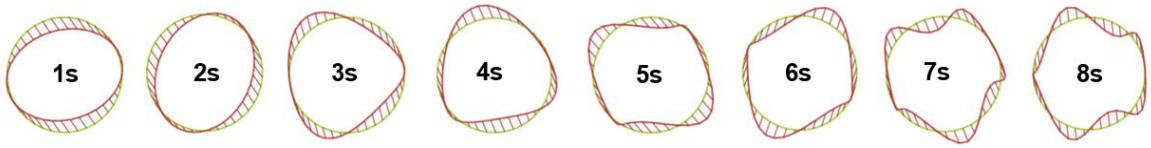

Figure 5: First *8* warping displacement profiles associated with shear modes.

3.1. Pre-Buckling Stresses

In order to perform GBT buckling analyses, it is mandatory to determine accurately the appropriate pre-buckling stresses (internal forces) caused by the applied loading. In the present formulation, two type of applied loading, both associated with an uniform pressure p^0, are considered: (i) axial compression ($W_1^{\sigma xx}$), applied at the end caps, and (ii) lateral compression ($W_a^{\sigma\theta\theta}$), applied around the lateral wall and normal to it – they may act either alone (*e.g.*, in pipes) or in combination (*e.g.*, in tanks), but always dependent on a single load parameter λ. Using (20) and (27), and introducing the displacement profiles of modes **a** ($u_a=0$, $v_a=0$ and $w_a=1$) and **1** ($u_1=1$) in (30) to (33), one obtains the pre-buckling stresses and corresponding resultants (i) for lateral compression (j=**a**),

$$\sigma_{\theta\theta}^{0} = Q_{22}\left(\frac{w_a}{r}\right)\phi_a^0 = Q_{22}\left(\frac{1}{r}\right)\phi_a^0$$

$$W_a^{\sigma\theta\theta} = B_{aa}\phi_a^0$$

$$\sigma_{\theta\theta}^{0} = \frac{Q_{22}}{r}\left(\frac{W_a^{\sigma\theta\theta}}{B_{aa}}\right) \quad , \quad (49)$$

where

$$B_{aa} = \oint \frac{A_{22}}{r} d\theta \quad (50)$$

$$W_a^{\sigma\theta\theta} = 2\pi r p^0 \quad (51)$$

and (ii) for longitudinal compression (j=**1**),

$$\sigma_{xx}^{0} = Q_{11}u_1\phi_{1,xx}^0 = Q_{11}\phi_{1,xx}^0$$

$$W_1^{\sigma xx} = C_{11}\phi_{1,xx}^0$$

$$\sigma_{xx}^{0} = Q_{11}\frac{W_1^{\sigma xx}}{C_{11}} \quad , \quad (52)$$

where

$$C_{11} = \oint A_{11} r d\theta \quad (53)$$

$$W_1^{\sigma xx} = \pi r^2 p^0 \quad . \quad (54)$$

Thus, it is possible to rewrite the pre-buckling stresses as functions of their resultants, through the elimination of the amplitude functions ϕ (see Eqs. (49) and (52)). Then, incorporating these pre-buckling stress representations into Eqs. (28)-(29) and (45)-(46) leads to the geometric stiffness matrices

$$X_{jik}^{\sigma xx} = \frac{W_1^{\sigma xx}}{C_{11}} \oint A_{11}\left(w_k w_i + \frac{1}{4}\left(v_k - \frac{u_{k,\theta}}{r}\right)\left(v_i - \frac{u_{i,\theta}}{r}\right)\right) r d\theta \quad (55)$$

$$X_{jik}^{1\sigma\theta\theta} = \frac{W_a^{\sigma\theta\theta}}{B_{aa}} \oint A_{22}\left(\frac{v_k - w_{k,\theta}}{r}\right)\left(\frac{v_i - w_{i,\theta}}{r}\right) d\theta \quad X_{jik}^{2\sigma\theta\theta} = \frac{W_a^{\sigma\theta\theta}}{B_{aa}} \oint \frac{A_{22}}{4}\left(v_k - \frac{u_{k,\theta}}{r}\right)\left(v_i - \frac{u_{i,\theta}}{r}\right) d\theta \quad (56)$$

and also to the matrices stemming from the work done by the follower external pressure,

$$H_{ik}^{1} = \frac{W_a^{\sigma\theta\theta}}{r B_{aa}} \oint A_{22} w_k u_i d\theta \quad (57)$$

$$H_{ik}^{2} = \frac{W_a^{\sigma\theta\theta}}{r B_{aa}} \oint A_{22}\left(\frac{w_{k,\theta} - v_k}{r}\right) v_i d\theta \quad . \quad (58)$$

4. Numerical Solution (Beam Finite Element Formulation)

After incorporating the cross-section mechanical, geometric and follower pressure properties into the variational equation (see (18), (22), (23) and (44)), one is lead to

$$\int_L (C_{ik}\phi_{k,xx}\delta\phi_{i,xx} + D^1_{ik}\phi_{k,x}\delta\phi_{i,x} + D^2_{ik}\phi_k\delta\phi_{i,xx} + D^2_{ki}\phi_{k,xx}\delta\phi_i + B_{ik}\phi_k\delta\phi_i + \\ + X^{\sigma xx}_{jik}\phi_{k,x}\delta\phi_{i,x} + X^{1\sigma\theta\theta}_{jik}\phi_k\delta\phi_i + X^{2\sigma\theta\theta}_{jik}\phi_{k,x}\delta\phi_{i,x} + H^1_{ik}\phi_{k,x}\delta\phi_{i,x} + H^2_{ik}\phi_k\delta\phi_i)dx \quad , \quad (59)$$

a system of equilibrium equations (one per deformation mode) that, together with the members support conditions (written in modal form), defines a *one-dimensional* eigenvalue problem expressed in terms of the modal amplitude functions $\phi_k(x)$. The solution of this problem consists of the member bifurcation pressure values (eigenvalues) and corresponding buckling mode shapes (eigenvectors).

The buckling analysis is performed by means of a GBT-based beam finite element formulation similar to that recently developed and implemented by Basaglia *et al.* (2015) – the main steps and procedures involved in formulating this beam finite element are the following:

(i) Approximate the modal amplitude functions $\phi_k(x)$ by means of linear combinations of (i_1) Lagrange cubic polynomial primitives (axial extension and warping shear deformation modes, *i.e.*, those involving exclusively out-of-plane/warping displacements u) and (i_2) Hermite cubic polynomials, (remaining deformation modes: shell-type, axis-symmetric and torsion). Then, one has

$$\phi_k(x) = \Psi_\alpha(\xi)d^{e.i}_{k\alpha} = \Psi_1 d^{e.i}_{k1} + \Psi_2 d^{e.i}_{k2} + \Psi_3 d^{e.i}_{k3} + \Psi_4 d^{e.i}_{k4} \quad , \quad (60)$$

where (i_1) $d^{e.i}_{k\alpha}$ are the generalised displacements of finite element i and (i_2) Ψ_α are either Lagrange cubic polynomial primitives or Hermite polynomials, expressed as

$$\Psi_{1,x} = \tfrac{1}{2}(1-\xi)(3\xi-1)(3\xi-2) \qquad \Psi_{2,x} = \tfrac{9}{2}\xi(\xi-1)(3\xi-2)$$
$$\Psi_{3,x} = \tfrac{9}{2}\xi(1-\xi)(3\xi-1) \qquad \Psi_{4,x} = \tfrac{1}{2}\xi(3\xi-1)(3\xi-2) \quad (61)$$

$$\Psi_1 = L_e(\xi^3 - 2\xi^2 + \xi) \qquad \Psi_2 = (2\xi^3 - 3\xi^2 + 1)$$
$$\Psi_3 = L_e(\xi^3 - \xi^2) \qquad \Psi_4 = (3\xi^2 - 2\xi^3) \quad . \quad (62)$$

with $\xi = x/L_e$ (L_e is the finite element length).

(ii) Ensure satisfaction of the compatibility conditions (ii_1) $d^{e.i-1}_{k.3} = \phi_{k,x}(L_e) + d^{e.i}_{k.1} = \phi_{k,x}(0)$, and ($ii_2$) $d^{e.i-1}_{k.4} = \phi_k(L_e) + d^{e.i}_{k.2} = \phi_k(0)$. Then, the finite element modal generalized displacement vector is

$$d^{(e)}_k = \left[\, d_{k1} \quad d_{k2} \quad d_{k3} \quad d_{k4} \,\right]^{\mathrm{T}} \quad . \quad (63)$$

(iii) Write the finite element (iii_1) linear and geometric stiffness matrices, and the (iii_1) the matrices stemming from the work done by the follower external pressure as

$$K^{(e)}_{ik\alpha\beta} = C_{ik}\int_{L_e}\Psi_{\alpha,xx}\Psi_{\beta,xx}dx + B_{ik}\int_{L_e}\Psi_\alpha\Psi_\beta dx + D^1_{ik}\int_{L_e}\Psi_{\alpha,x}\Psi_{\beta,x}dx + \\ + D^2_{ik}\int_{L_e}\Psi_{\alpha,xx}\Psi_\beta dx + D^2_{ki}\int_{L_e}\Psi_\alpha\Psi_{\beta,xx}dx \quad (64)$$

$$G_{ik\alpha\beta}^{(e)} = X_{1ik}^{\sigma xx} \int_{L_e} \Psi_{\alpha,x} \Psi_{\beta,x} dx + X_{aik}^{1\sigma\theta\theta} \int_{L_e} \Psi_\alpha \Psi_\beta dx + X_{aik}^{2\sigma\theta\theta} \int_{L_e} \Psi_{\alpha,x} \Psi_{\beta,x} dx \quad (65)$$

$$H_{ik\alpha\beta}^{(e)} = H_{ik}^{1} \int_{L_e} \Psi_{\alpha,x} \Psi_{\beta,x} dx + H_{ik}^{2} \int_{L_e} \Psi_\alpha \Psi_\beta dx \quad , \quad (66)$$

where the roman $(1, a, i, k)$ and greek (α, β) subscripts identify the *deformation mode* and *degree of freedom* (modal generalized displacement), respectively.

(iv) Take into account the member *support conditions*, expressed in terms of the modal degrees of freedom (usually modal amplitude values and/or derivatives at the member ends – see (60)), perform the assembly procedure leading to the discretized eigenvalue problem

$$([K] - \lambda([G] + [H]))\{d\} = \{0\} \quad , \quad (67)$$

where (iv$_1$) $[K]$ and $[G]$ are the member linear and geometrical stiffness matrices, (iv$_2$) $[H]$ is the matrix stemming from the work done the follower external pressure, (iv$_3$) λ is the load parameter (all applied pressures depend linearly on λ) and (iv$_4$) $\{d\}$ is the generalized modal amplitude vector – its components are the (unknown) values and/or derivatives of the GBT deformation mode amplitudes at the member nodes (finite element end cross-sections).

5. Illustrative Examples

In order to validate and illustrate the application and capabilities of the proposed GBT formulation and numerical implementation, results concerning the elastic buckling behavior of several circular cylindrical steel shells acted by external pressure are presented and discussed next. The validation of the GBT-based results (critical buckling pressures and mode shapes) is made through the comparison with values either available in the literature or obtained through ANSYS (SAS 2009) shell finite element analyses – the cylindrical shells are discretized by means of refined meshes of SHELL181 elements, which account for distributed pressure follower effects and are employed with a "full integration" option.

5.1. Simply Supported Cylindrical Shells under Lateral External Pressure

The first illustrative example concerns the buckling behavior of simply supported (end cross-sections able to warp freely, restrained against radial and tangential displacements and having the corresponding rotations free) steel ($E=200\,GPa$ and $\nu=0.3$) cylindrical shells acted by uniform lateral external pressure (*i.e.*, only $\sigma_{\theta\theta}^{0}$) and exhibiting a wide range of geometrical parameters: $0.5 < L/r < 5$ and $300 < r/t < 3000$ (*14* different cases)[7]. The GBT results obtained are compared with the buckling pressure values (p_{cr}) and number of lobes (n_{cr}) reported by Vodenitcharova & Ansourian (1996), obtained by solving Flügge's stability equations (expressed in coupled form – Flügge 1973) and provided in Table 1[8]. Figure 6 shows the buckled mid-span cross-sections determined by means of GBT analyses for the shells corresponding to cases *5, 9 11* and *13*.

The observation of the results displayed in Table 1 shows that there is an excellent agreement between the critical buckling pressures provided by the GBT analyses and those reported by the above authors. Indeed, the average difference between the two sets of p_{cr} values is *1.6%*, with a maximum of *3.9%*, occurring for the shortest and thickest cylinder (case 1). Moreover, as it would be logical to expect, the number of critical buckling mode lobes (n_{cr}) was found to decreases as t and/or L increase.

[7] In the present study, the length $L=600cm$ was always adopted.

[8] Flugge's stability equations (i) are based on the assumption that the in-plane displacement are not negligible in comparison with the transverse deflections and (ii) consider an external pressure acting always normally to the shell (deformed) surface.

Table 1: Critical buckling pressures and mode lobe numbers of cylindrical shells under lateral external pressure.

			Present Study			*Vodenitcharova & Ansourian (1996)*		
Case	*L/r*	*r/t*	*GBT mode*[9]	n_{cr}	$p_{cr} \times 10^{-4}$ *(MPa)*	n_{cr}	$p_{cr} \times 10^{-4}$ *(MPa)*	Δ *(%)*
1	*0.5*	*300*	*30*	*15*	*2873.541*	*15*	*2766.2*	*3.9*
2	*0.5*	*3000*	*56*	*28*	*8.018*	*28*	*7.816*	*2.6*
3	*1*	*300*	*22*	*11*	*1307.456*	*11*	*1269.6*	*3.0*
4	*1*	*500*	*26*	*13*	*356.761*	*13*	*348.43*	*2.4*
5	*1*	*1000*	*30*	*15*	*61.865*	*15*	*60.488*	*2.3*
6	*1*	*1500*	*34*	*17*	*22.110*	*17*	*21.767*	*1.6*
7	*1*	*2000*	*36*	*18*	*10.723*	*18*	*10.559*	*1.6*
8	*1*	*3000*	*40*	*20*	*3.859*	*20*	*3.81*	*1.3*
9	*2*	*300*	*16*	*8*	*617.643*	*8*	*607.33*	*1.7*
10	*2*	*3000*	*28*	*14*	*1.898*	*14*	*1.884*	*0.7*
11	*3*	*300*	*14*	*7*	*409.624*	*7*	*407.19*	*0.6*
12	*3*	*3000*	*24*	*12*	*1.255*	*12*	*1.251*	*0.3*
13	*5*	*300*	*10*	*5*	*237.007*	*5*	*235.34*	*0.7*
14	*5*	*3000*	*18*	*9*	*0.746*	*9*	*0.744*	*0.2*

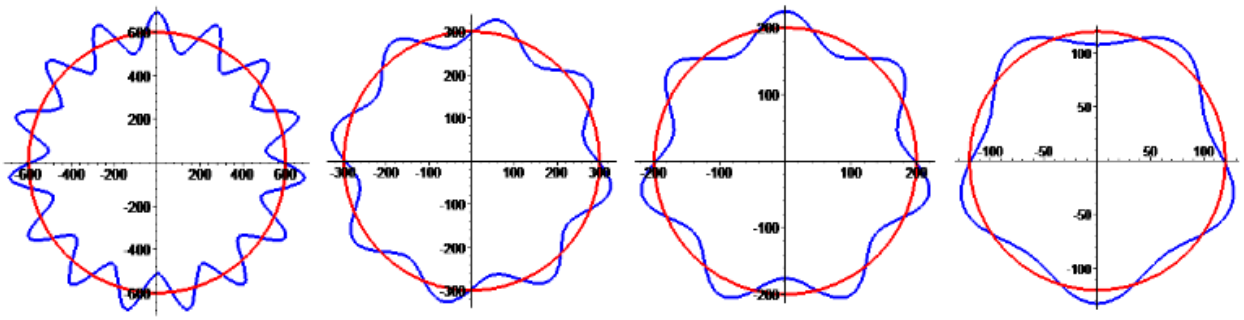

Case *5* (n_{cr}=*15*) Case *9* (n_{cr}=*8*) Case *11* (n_{cr}=*7*) Case *13* (n_{cr}=*5*)

Figure 6: Critical buckling mode shapes of the cylindrical shell corresponding to cases *5*, *9*, *11* and *13*.

5.2. Influence of the Follower External Pressure

The influence of the follower external pressure in the buckling behavior of pipes is investigated in this section. In long pipes subjected to (uniform) lateral external pressure, the critical buckling value depends on the nature of such pressure, *i.e.*, on whether it is *non-conservative* (deformation-dependent – follower) or *conservative* (deformation-independent). For each case, the critical buckling pressure value is given, respectively, by the expressions (Iwata *et al.* 1991)

$$p_{cr.1} = \frac{E}{1-\nu^2}\frac{t^3}{4r^3} \qquad \text{(deformation-dependent pressure)} \tag{68}$$

[9] Shear modes may also have a very small participation in the shell critical buckling mode configuration.

$$p_{cr.2} = \frac{E}{1-\nu^2}\frac{t^3}{3r^3} \qquad \text{(deformation-independent pressure)} \qquad , \quad (69)$$

and corresponds to an oval buckling mode (which is the critical one only in long pipes).

Consider now thin-walled steel ($E=210\,GPa$ and $\nu=0.3$) cylindrical pipes with lengths $L=20,50cm$ (short pipes) and $L=400cm$ (long pipe), radius $r=6cm$ and wall thickness $t=0.12cm$. The pipes are (locally and globally) simply supported and acted by an uniform lateral external pressure p. Initially, two GBT analyses are carried out, namely (i) *GBT-1*, which takes into account the follower pressure effects, and (ii) *GBT-2*, which disregards such effects (*i.e.*, matrix [*H*] is null in Eq. (67)). Then, two ANSYS shell finite element analyses are performed, one modeling the pipe by means of SHELL181 elements and the other adopting a pipe discretization into a SHELL63 element mesh. Table 2 shows the pipe buckled mid-span cross-sections associated with the two external pressure natures and provides the associated critical buckling pressures yielded by (i) Eqs. (68)-(69), (ii) GBT analyses and (iii) ANSYS shell finite element analysis analyses – *CASE A* and *CASE B* correspond the application of non-conservative and conservative lateral external pressure, respectively. The comparison of the various sets of buckling results lead to the following conclusions:

(i) There is a very good agreement between the GBT results and the values either yielded by the analytical expressions (long pipes) or obtained from the ANSYS shell finite element analyses.

(ii) Although the pipe buckling mode shapes concerning *CASE A* and *CASE B* are very similar (virtually identical), the corresponding critical buckling pressures are visible different – those associated with

Table 2: Critical buckling pressures (*MPa*) and buckled mid-span cross-sections of pipes under lateral external pressure.

	CASE A – non-conservative pressure			*CASE B – conservative pressure*		
L (*cm*)	$p_{cr.1}$ *Eq. (68)*	*GBT-1*	*ANSYS* (*SHELL181*)	$p_{cr.2}$ *Eq. (69)*	*GBT-2*	*ANSYS* (*SHELL63*)
20	-	*3.4149* 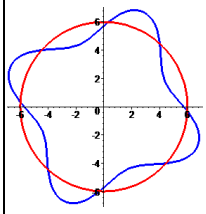	*3.4232* 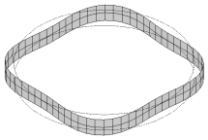	-	*3.5273* 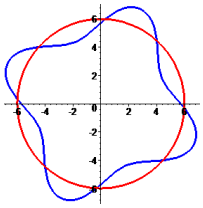	*3.5634* 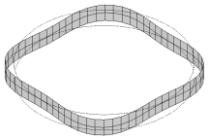
50	-	*1.4097* 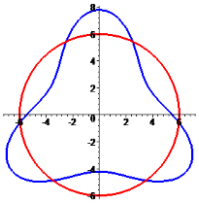	*1.4184* 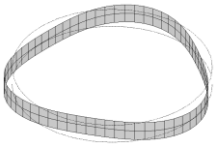	-	*1.5742* 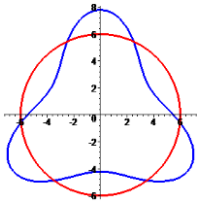	*1.5712* 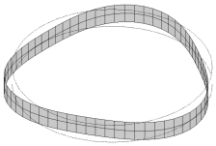
400	*0.4615* 	*0.4624* 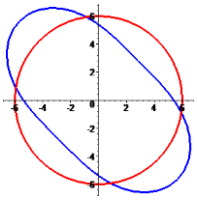	*0.4659* 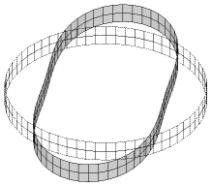	*0.6154* 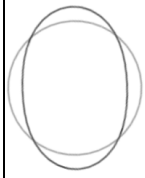	*0.6165* 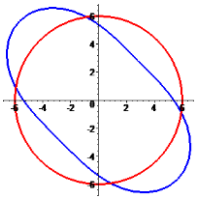	*0.6176* 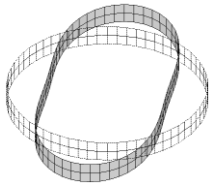

the application of a follower external pressure (*CASE A*) are always smaller, which means that neglecting the follower pressure effects leads to critical buckling pressure overestimations.

(iii) The follower pressure effects are more pronounced for the pipes buckling in modes with small lobe numbers. Indeed, the percentage differences between the critical buckling pressures concerning *CASE A* and *CASE B* are equal to *3*%, *12*% and *33*% for $n_{cr}=4$ (*L=20cm*), $n_{cr}=3$ (*L=50cm*) and $n_{cr}=2$ (*L=400cm*), respectively. This stems from the fact that a lower lobe number is associated with a buckling mode shape "more distant" from the pipe undeformed (cylindrical) configuration, *i.e.*, involving larger changes in wall orientation, which are at the root of the follower pressure effects. Indeed, the relevance of such effects drops as the buckled cross-section configuration becomes closer to the circular shape, which is the case when the number of lobes grows (their amplitude decreases).

5.3. Two-Span Pipe under Lateral External Pressure

Attention is now turned to assessing the buckling behavior of two-span steel (*E=210 GPa* and *v=0.3*) pipes acted by uniform lateral external pressure. As shown in Figure 7, the pipe end cross-sections are locally and globally fixed (fully restrained against radial, tangential and longitudinal displacements and rotations) and the intermediate clamp-type support restrains all cross-section in-plane (radial and tangential), while there is warping and rotation continuity. The pipes exhibit a circular hollow cross-section with radius *r=6cm* and thickness *t=0.12cm*, and the two equal spans have length *L*.

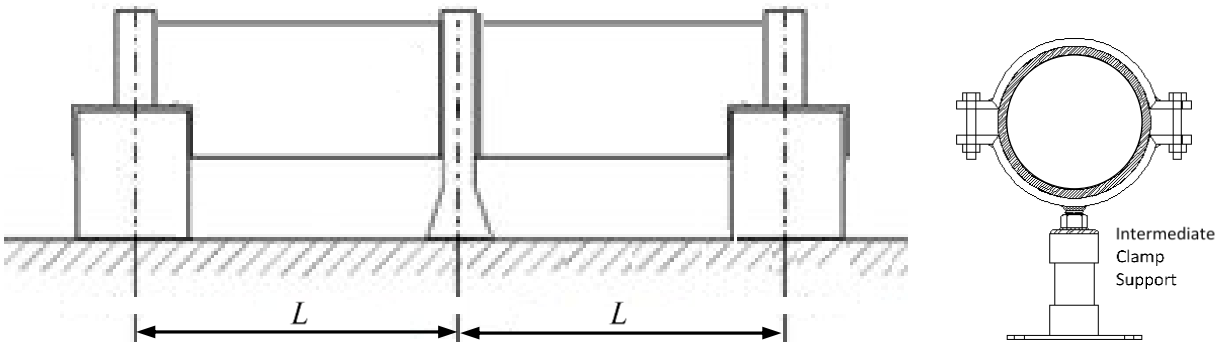

Figure 7: Two-span pipe under lateral external pressure.

Table 3 shows the pipe critical buckling pressures and mode lobe numbers obtained through beam (GBT) and shell (ANSYS) finite element analyses. While the GBT finite element analyses involve a pipe longitudinal discretization into *12* beam elements (*6* in each span) and include *7* deformation modes (**2**+**4**+**6**+**8**+**10**+**12**+**14**), which amounts to a total of *217* degrees of freedom, the ANSYS shell finite element analyses involved a pipe discretization into fairly refined meshes associated with a number of degrees of freedom varying between *11500* (*L=10cm*) to *150000* (*L=200cm*). Although no special effort was made to minimise/optimize the shell finite element discretization, it is clear that the numbers of degrees of freedom involved in the two approaches are orders of magnitude apart. This difference is even more striking if one realizes that it is possible to include in the GBT analyses only a fairly small fraction (appropriately selected, of course) of the deformation modes determined. As for Figure 8, it displays pairs of critical buckling mode configuration views, obtained from ANSYS analyses, for *L=10,35,100cm* pipes.

The observation of the results displayed in Table 3 and Figure 8 shows that there is a virtual coincidence between the critical buckling pressures yielded by the GBT and ANSYS analyses (all differences below *4.0%*). Moreover, there is also very close agreement between the buckling mode shapes provided by two types of analysis.

Table 3: GBT and ANSYS critical buckling pressures and mode lobe numbers.

L (cm)	*GBT mode*	n_{cr}	$p_{cr.GBT}$ (MPa)	$p_{cr.ANSYS}$ (MPa)	Δ (%)
10	*12*	*6*	*8.971*	*8.640*	*-3.8*
15	*10*	*5*	*5.849*	*5.671*	*-3.2*
25	*8*	*4*	*3.356*	*3.233*	*-3.8*
35	*6*	*3*	*2.503*	*2.436*	*-2.8*
50	*6*	*3*	*1.591*	*1.580*	*-0.7*
100	*4*	*2*	*0.737*	*0.729*	*-1.1*
150	*4*	*2*	*0.518*	*0.521*	*0.5*
200	*4*	*2*	*0.482*	*0.484*	*0.4*

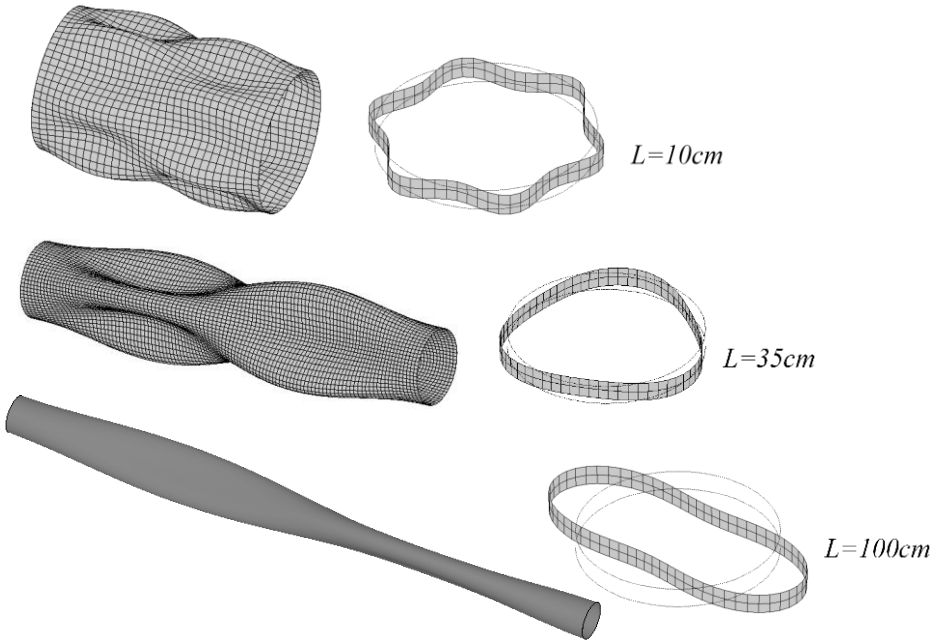

Figure 8: ANSYS critical buckling mode configurations of pipes with *L=10,35,100cm.*

5.4. Pressure Vessels

Lastly, steel (*E=210GPa* and *v=0.3*) simply supported pressure vessels (end sections locally/globally pinned and free to warp[10]) with lengths *L=200cm* and *L=400cm* are analyzed. The pressure vessels (i) have a circular hollow cross-section with radius *r=200cm* and three thickness values, namely *t=1*, *2* or *3cm*, (ii) exhibit flat circular end surfaces and (ii) are subjected to either hydrostatic pressure (*i.e.*, external pressure acting on all surfaces) or lateral external pressure alone (no pressure on the flat end surfaces). While Table 4 provides the critical buckling pressures and mode lobe numbers obtained by means of the beam (GBT) and shell (ANSYS) finite element analyses, Figure 9 shows two pairs of critical buckling

[10] These may be seen as "artificial support conditions", since it is logically to expect the flat end surfaces to provide, at least, partial warping restraint to the vessel end cross-section walls – naturally, such warping restraint is extremely difficult to quantify. In practice, however, this warping restraint may be attenuated by the presence of fairly flexible rings capping the vessel end cross-section walls and acting as expansion joints. If this is case, the end support conditions assumed in the analyses carried out in this work become "more realistic".

Table 4: Pressure vessels: GBT and ANSYS critical buckling hydrostatic and lateral pressures and mode lobe numbers.

				Hydrostatic Pressure			*Lateral Pressure*	
L (*cm*)	t (*cm*)	*GBT mode*	n_{cr}	$p_{cr.Hy.GBT}$ (*MPa*)	$p_{cr.Hy.ANSYS}$ (*MPa*)	Δ (%)	$p_{cr.Lt.GBT}$ (*MPa*)	$\frac{p_{cr.Lt.GBT}}{p_{cr.Hy.GBT}}$
200	*1*	*20*	*10*	*0.370*	*0.361*	*2.4*	*0.400*	*1.08*
	2	*18*	*9*	*2.185*	*2.192*	*-0.3*	*2.321*	*1.06*
	3	*16*	*8*	*6.276*	*6.305*	*-0.4*	*6.613*	*1.04*
400	*1*	*14*	*7*	*0.183*	*0.182*	*0.9*	*0.189*	*1.03*
	2	*12*	*6*	*1.038*	*1.030*	*0.8*	*1.075*	*1.04*
	3	*10*	*5*	*2.943*	*2.956*	*-0.4*	*3.050*	*1.04*

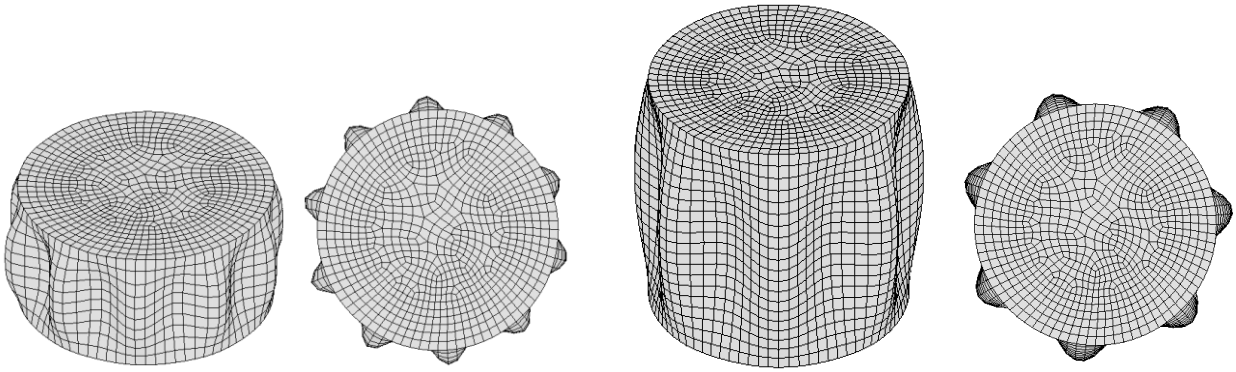

L=200cm *L=400cm*

Figure 9: ANSYS critical buckling mode configurations of pressure vessels with *t=1cm* under hydrostatic pressure.

mode shape views, obtained from ANSYS analyses of pressure vessels with *t=1cm* and *L=200cm* or *L=400cm*. In order assess and quantify the (detrimental[11]) effect of the longitudinal stress caused by the external pressure acting on the flat end surfaces), Table 4 presents also values of GBT-based critical buckling pressures obtained for cylindrical shells acted by external lateral pressure alone (*i.e.*, without the flat end surfaces). Once again, the GBT analyses involve only a small fraction of the number of degrees of freedom required by their ANSYS counterparts: *96* (*6* beam elements and modes **8**+**10**+**12**+**14**+**16**+**18**+**20**+**22**) versus *13800* (*L=200cm*) or *18600* (*L=400cm*). The analysis of the GBT and ANSYS buckling results presented prompts the following remarks:

(i) In spite of the huge difference in the numbers of degrees of freedom involved in the two analyses, the GBT and ANSYS critical buckling pressure are again extremely close – with one exception (the shortest and thinnest pressure vessel – *L=200cm* and *t=1cm*), all the differences are below *1%*.

(ii) The detrimental influence of the longitudinal compressive stresses, stemming from the hydrostatic pressure acting on the flat end surfaces, is slightly more pronounced for the longer pressure vessels – this feature has already reported, nearly two decades ago, by Koga & Morimatsu (1998). Nevertheless, the differences never exceeded *8%* in all the cases considered in this work.

(iii) All buckling mode exhibit minute end surface transverse displacements, which are not visible to the naked eye and occur mainly at the surface edge (due to warping displacement compatibility along the end wall contour[12]. Moreover, as in all the previous examples, the number of critical buckling mode lobes drops as the pressure vessel wall thickness and/or length increases.

[11] The additional compressive longitudinal stresses erode the pressure vessel wall bending stiffness, thus making it more prone to buckling caused by the external lateral pressure.

[12] The deformed mesh three-dimensional views depicted in Figure 9 may give the opposite (and wrong) idea.

6. Conclusion

This paper reported the development, finite element implementation and application of a GBT formulation intended to analyze the buckling behavior of circular cylindrical steel shells subjected to uniform external pressure. Initially, the GBT equilibrium equation system was established, incorporating (i) geometrical stiffness terms associated with the internal work done by the pre-buckling longitudinal and hoop stresses, and (ii) non-linear terms associated with effects stemming from the follower nature of the external lateral pressure. Then, a very brief review of the most relevant concepts involved in performing GBT buckling analyses of CHS members was provide, paying particular attention to (i) the cross-section analysis and (ii) the formulation and numerical implementation of a GBT-based beam finite element. Finally, the buckling behaviors of thin-walled steel pipes and pressure vessels acted by uniform external pressure were investigated. For validation purposes, some GBT results were compared with values either available in the literature or obtained by means of ANSYS shell finite element analyses. In spite of the huge disparity between the numbers of degrees of freedom involved in the two numerical analyses (orders of magnitude apart), an excellent agreement was found in all cases. Moreover, the results obtained made it possible (i) to show that the follower pressure effects are more pronounced for cylindrical shells buckling in modes with small lobe numbers, as well as to quantify those effects, and (ii) to assess the detrimental influence of the longitudinal compressive stresses (caused by the pressure applied on the flat end surfaces) on the buckling behavior of pressure vessels – it was found that such influence is slightly more marked in the shorter ones.

Acknowledgements

The financial support of *Fundo de Apoio ao Ensino, à Pesquisa e à Extensão* (FAEPEX-UNICAMP – Brazil), through project 0841/14, is gratefully acknowledged. The first and third authors also acknowledge the financial support provided respectively by (i) *Conselho Nacional de Desenvolvimento Científico e Tecnológico* (CNPq – Ministry of Science**,** Technology and Innovation of Brazil), through project nº 446679/2014-3, and (ii) FCT (*Fundação para a Ciência e a Tecnologia* – Portugal), through IDMEC, under LAETA, project UID/EMS/50022/2013.

References

Annaratone D (2007). *Pressure Vessel Design*, Springer-Verlag, Berlin.

Arjomandi K (2010). *Mechanical Response of Sandwich Pipes Subject to Hydrostatic Pressure and Bending*, Ph.D. Thesis, Department of Civil and Resource Engineering, Dalhousie University, Halifax, Canada.

Basaglia C, Camotim D, Silvestre N (2015). Buckling and vibration analysis of cold-formed steel CHS members and frames using generalized beam theory, *International Journal of Structural Stability and Dynamics*, **15** (8), 1540021-1 - 1540021-25.

Bebiano R, Gonçalves R, Camotim D (2015). A cross-section analysis procedure to rationalise and automate the performance of GBT-based structural analyses, *Thin-Walled Structures*, **92**(July), 29-47.

Bodner SR (1958). On the conservativeness of various distributed force systems, *Journal of the Aerospace Science*, **25**(2), 132-133.

Boresi AP (1955). A refinement of the theory of buckling of rings under uniform pressure, *Journal of Applied Mechanics*, **22**(1), 95-102.

Brendel B, Ramm E (1980). Linear and nonlinear stability analysis of cylindrical shells, *Computers & Structures*, **12**(4), 549-558.

Bryan GH (1889). Application of the energy test to the collapse of a long thin pipe under external pressure, *Cambridge Philosophical Society Proceedings*, **6**, 287-292.

Cao Q, Zhao Y (2010). Buckling strength of cylindrical steel tanks under harmonic settlement, *Thin-Walled Structures*, **48**(6), 391-400.

Flügge W (1973). *Stresses in Shells* (2nd edition), Springer Verlag, Berlin.

Hibbitt HD (1979). Some follower forces and load stiffness, *International Journal for Numerical Methods in Engineering*, **14**(6), 937-941.

Iwata K, Tsukimori K, Kubo F (1991). A symmetric load-stiffness matrix for buckling analysis, *International Journal of Pressure Vessels and Piping*, **45**(1), 101-120.

Karamanos S and Tassoulas J (1996). Tubular members I: stability analysis and preliminary results, *Journal of Engineering Mechanics* (ASCE), **122**(1), 64-71.

Koga T, Morimatsu S (1998). Bifurcation buckling of circular cylindrical shells under uniform external pressure, *American Institute of Aeronautics and Astronautics* (*AIAA*) *Journal*, **27**(2), 242-248.

Kyriakides S, Corona E (2007). *Mechanics of Offshore Pipelines – Vol. 1: Buckling and Collapse*, Elsevier, Oxford.

von Mises R (1929). Der kritische aussendruck für allseits belastete zylindrische rohre, *Fest Zum 70 Geburtstang von Prof. Dr. A. Stodola, Zürich*, 418-430 (also Translation Report No. 366, *U.S. Experimental Model Basin*, Washington D.C., 1933).

Nash WA (1954). Buckling of thin cylindrical shells subject to hydrostatic pressure, *Journal of the Aeronautical Sciences*, **21**(May), 354-355.

Paimushin VN. (2008). Static and dynamic beam forms of the loss of stability of a long orthotropic cylindrical shell under external pressure, *Journal of Applied Mathematics and Mechanics*, **72**(6), 738-747.

Paor C, Kelliher D, Cronin K, Wright WMD, McSweeney SG (2012). Prediction of vacuum-induced buckling pressures of thin-walled cylinders, *Thin-Walled Structures*, **55**(June), 1-10.

Rasheed HA, Yousif OH (2005). Stability of anisotropic laminated rings and long cylinders subjected to external hydrostatic pressure, *Journal of Aerospace Engineering* (ASCE), **18**(3), 129-138.

Ross CTF (2011). *Pressure Vessels: External Pressure Technology* (2nd edition), Woodhead Publishing Limited, Cambridge.

Sanders Jr. JL (1963). Non-linear theories for thin shells, *Quarterly of Applied Mathematics* **21** (1), 21-36.

SAS (Swanson Analysis Systems Inc.) (2009). *ANSYS Reference Manual* (version 12).

Schardt R (1989). *Verallgemeinerte Technishe Biegetheorie*, Springer-Verlag (Berlin). (German)

Silvestre N (2007). Generalised beam theory to analyse the buckling behaviour of circular cylindrical shells and tubes, *Thin-Walled Structures*, **45**(2) 185-198.

Vodenitcharova T, Ansourian P (1996). Buckling of circular cylindrical shells subject to uniform lateral pressure, *Engineering Structures*, **18**(8), 604-614.